








RESEARCH ARTICLE | JANUARY 24 2024

Four-wave mixing with anti-parity-time symmetry in hot ^{85}Rb vapor

Special Collection: [Non-Hermitian Photonics](#)

Ziqi Niu   ; Yue Jiang  ; Jianming Wen  ; Chuanwei Zhang  ; Shengwang Du  ; Irina Novikova 

 Check for updates

Appl. Phys. Lett. 124, 044005 (2024)

<https://doi.org/10.1063/5.0173354>



View
Online



Export
Citation

CrossMark



Applied Physics Letters

Special Topic:
Advances in Quantum Metrology

Submit Today

Four-wave mixing with anti-parity-time symmetry in hot ^{85}Rb vapor

Cite as: Appl. Phys. Lett. **124**, 044005 (2024); doi: [10.1063/5.0173354](https://doi.org/10.1063/5.0173354)

Submitted: 21 August 2023 · Accepted: 3 January 2024 ·

Published Online: 24 January 2024



View Online



Export Citation



CrossMark

Ziqi Niu,^{1,a)}  Yue Jiang,^{2,3}  Jianming Wen,⁴  Chuanwei Zhang,⁵  Shengwang Du,⁵  and Irina Novikova¹ 

AFFILIATIONS

¹Department of Physics, William & Mary, Williamsburg, Virginia 23187, USA

²JILA, National Institute of Standards and Technology and the University of Colorado, Boulder, Colorado 80309, USA

³Department of Physics, University of Colorado, Boulder, Colorado 80309, USA

⁴Department of Physics, Kennesaw State University, Marietta, Georgia 30060, USA

⁵Department of Physics, The University of Texas at Dallas, Richardson, Texas 75080, USA

Note: This paper is part of the APL Special Collection on Non-Hermitian Photonics.

a) Author to whom correspondence should be addressed: zniu01@wm.edu

ABSTRACT

We report an experimental demonstration of anti-parity-time symmetric optical four-wave mixing in thermal rubidium vapor, where the propagation of probe and Stokes fields in a double- Λ scheme is governed by a non-Hermitian Hamiltonian. We are particularly interested in studying quantum intensity correlations between the two fields near the exceptional point, taking into account loss and accompanied Langevin noise. Our experimental measurements of classical four-wave mixing gain and the associated two-mode relative-intensity squeezing are in reasonable agreement with the theoretical predictions.

Published under an exclusive license by AIP Publishing. <https://doi.org/10.1063/5.0173354>

While any Hermitian operator has real eigenvalues, being Hermitian is not a necessary condition for this property. Recent demonstrations have shown that any Hamiltonian \hat{H} either symmetric^{1–3} or anti-symmetric^{4,5} under joint parity-time ($\hat{P}\hat{T}$) transformations (with either $[\hat{H}, \hat{P}\hat{T}] = 0$ or $\{\hat{H}, \hat{P}\hat{T}\} = 0$, correspondingly) can still yield a real energy spectrum. Both types of systems undergo a phase transition in which the real eigenvalues of the Hamiltonian become imaginary at a singular point of the parameter space, known as an exceptional point (EP). Remarkably, even minimal perturbations of the interaction parameters in the vicinity of the EP may cause dramatic changes in the system observable behavior, enabling performance enhancement of various sensors^{6–9} and many other applications.¹⁰ The mathematical equivalence of Schrödinger equation and paraxial wave propagation equation in materials with complex refractive indices has paved the way for experimental realization of PT and anti-PT symmetric optical and photonic structures by leveraging the spatial variation of their optical properties. Notably, PT symmetric structures typically employ spatially interleaved gain and loss channels,^{3,11–13} enabling exciting possibilities for practical applications such as EP-enhanced sensing and PT symmetric lasers.^{14–19} However, unavoidable optical gain and loss pose challenges to many sensing schemes that hold great theoretical promise, since the associated Langevin noises

disrupt PT symmetry in the quantum regime.^{20,21} Contrarily, anti-PT symmetric systems offer a promising solution to this issue, as they can potentially be realized without loss or gain by solely manipulating the spatial variation of the real part of refractive indices.^{4,22,23}

Recently, a fascinating alternative realization of anti-PT symmetry, without the need for spatially alternating regions with different refractive indices, has been demonstrated in cold Rb atoms.²⁵ In this system, the coupling between two optical fields (referred to as probe and Stokes) is established via resonant four-wave mixing (FWM) with the help of two intense pump laser fields, and a nearly lossless propagation of a resonant field and tunable nonlinearity is achieved, thanks to strong coupling of light and long-lived ground-state atomic coherence under the conditions of electromagnetically induced transparency (EIT). By varying the nonlinearity strength, the system exhibited an anti-PT phase transition with the eigenvalues transforming from imaginary to real at the EP. However, implementing such a lossless FWM scheme in inhomogeneously broadened optical systems is challenging due to unavoidable residual absorption, even under the EIT resonances. Here, we recreated similar conditions for anti-PT symmetry breaking by operating away from exact optical transition, thus mitigating the adverse effects of inhomogeneous broadening. This allows us to use a Rb vapor cell and a single strong pump laser field, rather than a

cold atomic ensemble, which greatly reduces the complexity of the experiment and can operate in the continuous regime. This system also enables experimental studies of the quantum properties of anti-PT phase breaking by measuring intensity squeezing and entanglement of the two output optical fields.^{26–30} Theory predicts distinct behaviors in their quantum fluctuations near the EP, offering promising avenues for precision quantum sensing.^{31,32} This knowledge can be used to gain additional insight into the operation of a wide range of quantum sensors based on this FWM system.^{28,33–36} In this work, we first characterize the anti-PT features classically by tracking the FWM gain for both probe and Stokes optical fields and then present theoretical and experimental analysis of nonclassical correlations in their relative-intensity noise. We consider a more realistic scenario, accounting for residual optical loss and associated Langevin noise, which inevitably reshapes the emergence of the anti-PT phase transition and modifies squeezing attributes. Finally, we identify the parameter space where the distinct anti-PT breaking features around the EP can be observed more clearly.

Following previous work (e.g., Refs. 26,37–40), we model the four-wave mixing process at the $5^2S_{1/2}, F = 2, 3 \rightarrow 5^2P_{1/2}$ optical transition of ^{85}Rb using a double- Λ interaction scheme, as shown in Fig. 1(a). The pump laser (red) at angular frequency ω and Rabi frequency Ω couples atomic transitions $|1\rangle \rightarrow |3\rangle$ and $|2\rangle \rightarrow |3\rangle$ with respective detuning $\Delta_1 = 0.7$ and $\Delta_2 = \Delta_1 + \Delta_{HF} = 3.7$ GHz, where $\Delta_{HF} = 3.035$ GHz is the hyperfine splitting of the $5S_{1/2}$ ground state. The two output modes, Stokes ($\omega_s, \hat{a}_s^\dagger$) and probe (ω_p, \hat{a}_p), are assumed to only couple to the $|3\rangle \rightarrow |2\rangle$ and $|3\rangle \rightarrow |1\rangle$ transitions, correspondingly, and, under the two-photon resonance condition, to obey the energy conservation $2\omega = \omega_s + \omega_p$. Under the non-depleted pump approximation, the nonlinear FWM interaction between the

probe and Stokes field operators, \hat{a}_p and \hat{a}_s , is described by the following coupled equations:^{25,41}

$$i \frac{\partial}{\partial z} \begin{pmatrix} \hat{a}_p \\ \hat{a}_s^\dagger \end{pmatrix} = \begin{pmatrix} -\frac{\Delta k}{2} & -\kappa \\ \kappa & \frac{\Delta k}{2} \end{pmatrix} \begin{pmatrix} \hat{a}_p \\ \hat{a}_s^\dagger \end{pmatrix}, \quad (1)$$

where $\Delta k = 2k - (k_p + k_s) \cos \theta$ is the phase mismatch with k, k_p , and k_s being, respectively, the wave numbers of the pump, probe, and Stokes waves and $\theta = 0.39^\circ$ is the fixed misalignment angle [Fig. 1(b)]. Note that, unlike most previous FWM studies, we operate at non-zero Δk ; this is required for achieving anti-PT symmetric interaction and the existence of the EP. In simulation, we extract the Δk by fitting the classical gain data as its value can be effectively modified by the medium. At the two-photon resonance, $\kappa = gN/2c\Delta_2$ is a real and tunable parametric interaction amplitude with the optical transition coupling strength g , atomic density N , and speed of light in vacuum c .

Equation (1) clearly resembles the Schrödinger-like equation with an effective Hamiltonian,

$$\mathbb{H}_{\text{APT}} = \begin{pmatrix} -\frac{\Delta k}{2} & -\kappa \\ \kappa & \frac{\Delta k}{2} \end{pmatrix}, \quad (2)$$

that anti-commutes with the joint parity-time operator,²⁵ $\{\mathbb{H}_{\text{APT}}, \hat{P}\hat{T}\} = 0$. Since \mathbb{H}_{APT} (2) does not contain any gain or loss, the commutation relations remain intact, removing the need for any Langevin noise terms in Eq. (1).

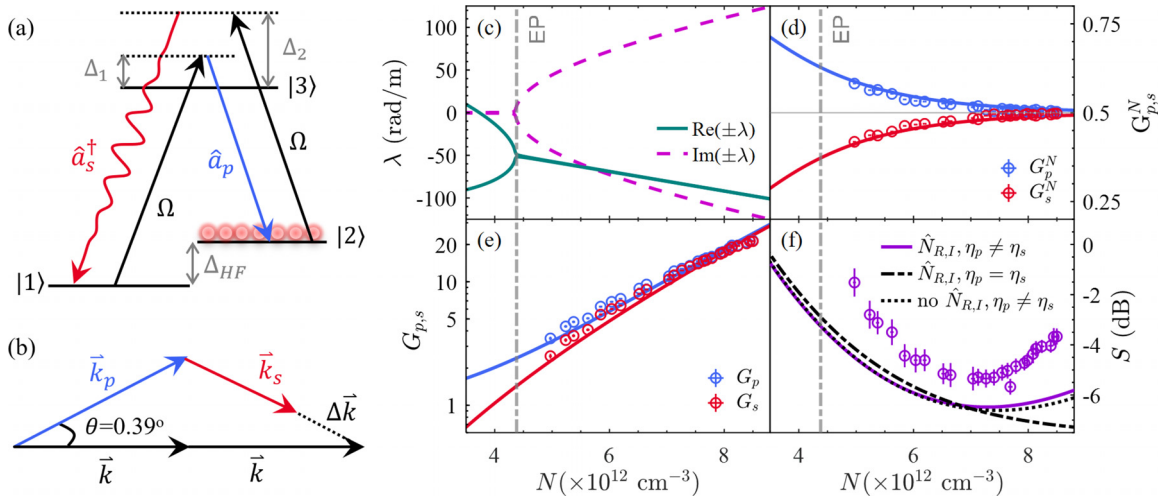


FIG. 1. (a) Interaction double- Λ scheme used for describing the four-wave mixing process at the D_1 transition of ^{85}Rb . Strong pump laser is detuned by $\Delta_1 = 0.7$ GHz and $\Delta_2 = 3.7$ GHz from the $5^2S_{1/2}, F = 2 \rightarrow 5^2P_{1/2}$ and the $5^2S_{1/2}, F = 3 \rightarrow 5^2P_{1/2}$ optical transitions, respectively. $\Delta_{HF} = 3035.7$ MHz is the ground-state hyperfine splitting. (b) Geometrical arrangement of the optical fields in the FWM process, showing the momentum mismatch $\Delta \vec{k} = 2\vec{k} - \vec{k}_p - \vec{k}_s$. (c) Anti-PT Hamiltonian eigenvalues $\pm \lambda$ vs atomic density N , calculated using experimental parameters. (d) and (e) Experimental (markers) and calculated (lines) absolute (e) and normalized (d) gain values for the probe and Stokes optical fields vs N . (f) Relative-intensity squeezing parameter S vs N , showing experimental data (markers) and simulated results from the full quantum model with imbalanced (solid line) detector efficiencies ($\eta_p = 78\%$ and $\eta_s = 83\%$), from the full quantum model with balanced (dash line) detector efficiencies ($\eta_p = \eta_s = 83\%$) and from the model included only imbalanced detector loss ($\eta_p = 78\%$ and $\eta_s = 83\%$, 100% transmission in atomic medium)²⁴ (dotted). In all cases, the imperfect detector efficiencies are accounted for using a beam splitter model. For (c)–(e), the dashed vertical lines indicate the predicted EP locations. Experimental parameters: $\theta = 0.39^\circ$, pump Rabi frequency $\Omega = 2\pi \times 0.42$ GHz, and cell length $z = 1.9$ cm. Temperature range: 100.5°C to 108.9°C , corresponding to the atomic density range of $N = 5 \times 10^{12}$ – 8.5×10^{12} cm^{-3} . Numerical model used $\Delta k = 210$ rad/m extracted from fitting experimental data (see the supplementary material).

The Hamiltonian (2) has two eigenvalues,

$$\pm\lambda = \pm \frac{\Delta k}{2} \sqrt{1 - \beta^2}, \quad (3)$$

where $\beta = |2\kappa/\Delta k|$ characterizes standard anti-PT features in parameter space: $\beta = 1$ indicates the EP of the regular anti-PT phase transition, marked by both eigenvalue and eigenstate coalescence. For $\beta < 1$, $\pm\lambda$ is real, placing the system in the anti-PT phase-broken regime; $\beta > 1$ yields imaginary $\pm\lambda$, preserving anti-PT symmetry. In addition to the aforementioned anti-PT phase transition with $\pm\beta$, we also expect clear variations of quantum properties of the probe and Stokes fields after interaction with the atomic medium. These variations depend on a transfer matrix connecting output fields at $z = L$ to their corresponding inputs at $z = 0$,

$$\begin{pmatrix} \hat{a}_p(L) \\ \hat{a}_s^\dagger(L) \end{pmatrix} = e^{-iH_{\text{APT}}L} \begin{pmatrix} \hat{a}_p(0) \\ \hat{a}_s^\dagger(0) \end{pmatrix} = \begin{pmatrix} A & C^* \\ C & A^* \end{pmatrix} \begin{pmatrix} \hat{a}_p(0) \\ \hat{a}_s^\dagger(0) \end{pmatrix}, \quad (4)$$

where $A = \cos(\lambda L) + i \sin(\lambda L)/\sqrt{1 - \beta^2}$ and $C = -i\beta \sin(\lambda L)/\sqrt{1 - \beta^2}$ with $|A|^2 - |C|^2 = 1$. To evaluate the potential of practical realization of anti-PT symmetry breaking, we focus on two experimentally observed parameters: the gain coefficients and relative-intensity fluctuations of the strongly correlated probe and Stokes fields for the different β values; we compare their behavior with the prediction of the ideal double- Λ system, considered earlier.

We first examine the classical traits of anti-PT behavior using probe and Stokes field gain values. We define the gain as the ratio of the measured output power to the input power of the seeded input field, $G_j = \langle \hat{n}_j(L) \rangle / \langle \hat{n}_{\text{seed}}(0) \rangle$ ($j = p, s$), where $\hat{n}_j = \hat{a}_j^\dagger \hat{a}_j$ is the photon-number operator. For weak probe seeding $\langle \hat{n}_p(0) \rangle$, as per Eq. (4), probe and Stokes gains become $G_p = |A|^2$ and $G_s = |C|^2$, respectively. We then can define normalized gains G_p^N and G_s^N as

$$\begin{aligned} G_p^N &= \frac{G_p}{G_p + G_s} = \frac{|A|^2}{|A|^2 + |C|^2}, \\ G_s^N &= \frac{G_s}{G_p + G_s} = \frac{|C|^2}{|A|^2 + |C|^2}. \end{aligned} \quad (5)$$

For $\beta > 1$, both output fields grow exponentially due to the presence of imaginary components in the eigenvalues. Since $|A|^2 \approx |C|^2$ for larger β , the two powers increase at a similar rate, and both G_p^N and G_s^N tend to converge to 0.5. Below the EP ($\beta < 1$), coherent power oscillations emerge in both fields. Moreover, as β varies, normalized gain for one field increases, while that for the other goes down; for $\beta \rightarrow 0$, weak FWM strength results in $|A|^2 \rightarrow 1$ and $|C|^2 \rightarrow 0$.

Given the proven capability of this experimental system to generate strong quantum correlations and entanglement between probe and Stokes fields,^{26,27,38} it is an ideal platform for investigations of the quantum aspects of an anti-PT symmetric system by monitoring the reduction of the relative-intensity fluctuations between the two fields below the shot noise level. This reduction is described by the squeezing parameter S , which is determined as a relative variance of the probe-Stokes intensity difference after the cell (at $z = L$),²⁴ normalized to their shot noise,

$$S = \frac{\text{Var}(\hat{n}_p - \hat{n}_s)}{\langle \hat{n}_p \rangle + \langle \hat{n}_s \rangle} = \frac{1}{|A|^2 + |C|^2}, \quad (6)$$

with detailed calculations provided in the supplementary material. In this ideal case, it is easy to predict the quantum noise behavior. When $\beta < 1$, S follows sinusoidal oscillations of the classical relative gains, occasionally dropping below the shot noise (when the output powers of the probe and Stokes fields become equal), indicating the emergence of moderate quantum squeezing. However, when $\beta > 1$, S monotonically decreases, implying growing quantum correlations in relative photon-number fluctuations. A larger κ corresponds to better intensity squeezing. Near the EP, S can display rapid variations as $\beta \rightarrow 1$, offering intriguing opportunities for quantum sensing.³¹ In practice, however, optical loss and imperfect detection efficiency limit the achievable squeezing level, and any further growth in κ only leads to deterioration of squeezing and eventually excess noise. Thus, to capture the experimental realities, we develop a model that incorporates the effects of these imperfections, as detailed in the supplementary material.

To control the value of β in our experiment, we choose to vary κ by manipulating either the atomic density N or the Rabi frequency Ω of the pump laser, keeping Δk fixed. The details of the experimental setup are provided in the supplementary material and in Refs. 34 and 42. In this work, most experimental parameters, such as pump laser frequency and Rabi frequency, and two-photon detuning $\delta = \omega - \omega_p - \Delta_{\text{HF}} = \omega_s - \omega - \Delta_{\text{HF}}$ have been optimized to maximize the relative-intensity squeezing for different atomic densities. Parameters used for the numerical simulations are derived from independent experimental characterizations. Since in our model, we do not take into account the detailed hyperfine structure of ⁸⁵Rb D₁ line, the theoretically predicted values for the two optimal two-photon detunings ($\delta \approx -28$ MHz for maximum squeezing and -17 MHz for highest gain) differ from the corresponding experimentally measured ones (1 and 12 MHz). Note, however, that in both cases, these values are 11 MHz apart from each other.

Figures 1(c)–1(f) present the variation of the classical and quantum characteristics of the probe and Stokes fields during the anti-PT phase transition as functions of N . Figure 1(c) shows the calculated real (green) and imaginary (purple) components of $\pm\lambda$. Under the given experimental conditions, the real part of λ_{\pm} above EP does not completely disappear, as expected in the ideal anti-PT scenario. This non-vanishing deviation is caused by additional imaginary contribution α to the diagonal term of the matrix [see Eq. (7)], introduced to account for residual optical losses for the probe field. Nonetheless, its presence does not fundamentally disrupt the optical field dynamics and, under certain conditions, does not significantly deteriorate the expected application performance. Figures 1(d) and 1(e) depict the net gains, $G_p = |A|^2$ and $G_s = |C|^2$, along with the normalized gains, $G_{p,s}^N$, for the probe and Stokes fields, respectively. Both numerical simulations and experimental data exhibit close agreement. Notably, we do not observe any oscillations in the probe and Stokes fields power below EP; instead, the output power of the seeded probe field gradually decreases, while the generated Stokes field slowly grows. In principle, right after the EP, their normalized gains rapidly converge to 0.5 as the two optical fields tend to equate and grow together, signifying the system's transition into the unbroken domain of the anti-PT phase. Before EP, oscillatory conversion between probe and Stokes is anticipated in the low-atomic-density region for small κ , stemming from spontaneous symmetry breaking. However, observing these periodic oscillations as well as rapid convergence requires longer optical path L (as discussed later) or a significantly larger phase mismatch Δk . Under

these conditions, the FWM gain below the EP is very low, posing experimental challenges. While understanding of this FWM gain dependence on Rb density does not require analysis of its internal symmetries, casting it in light of anti-PT symmetry breaking provides valuable insight into the principle characteristics of the two distinct regimes. For instance, it provides a clear distinction between energy-conserving probe-Stokes propagation once the anti-PT symmetry is broken and the common-mode amplification in the anti-PT symmetric regime. Also, this allows for straightforward prediction of the experimental conditions corresponding to the EP, where the system can exhibit maximum sensitivity to its parameter variations. The anti-PT symmetry analysis also connects the experimental observation to the broader field of non-Hermitian physics.

Figure 1(f) presents the experimentally measured relative-intensity squeezing parameter S as well as its numerical simulations for various scenarios. The solid line shows the predictions of the full theoretical model that assumes the experimentally measured imbalance between probe and Stokes detection efficiencies. For completeness, we also plot the model predictions for the case of the identical detector efficiency, shown as a dashed line. The dotted line gives the predictions of a simplified calculation²⁴ that neglects the atomic Langevin noise correction terms ($\hat{\mathbb{N}}_{R,I}$). As previously mentioned, in an ideal case, quantum correlations between the probe and Stokes intensify with increasing N . However, as shown here, in reality, the squeezing parameter S reaches its optimal value of ≈ 5 dB at a certain N , above which quantum correlations continuously deteriorate. This shift primarily originates from residual optical loss (particularly for the probe field) that increases quantum noise of each individual optical field and detector losses that hamper fully capturing the generated relative-intensity squeezing.

In the numerical model, a non-negligible $-\alpha$ appears in the relevant diagonal term of \mathbb{H}_{APT} in Eq. (1), representing the effective loss rate for the probe field amplitude. The presence of α unavoidably modifies the Heisenberg equations of motion Eq. (1), requiring adding undesirable Langevin noise and rendering them to

$$i\partial_z \begin{pmatrix} \hat{a}_p \\ \hat{a}_s^\dagger \end{pmatrix} = \begin{pmatrix} -\frac{\Delta k}{2} - i\alpha & -\kappa \\ \kappa & \frac{\Delta k}{2} \end{pmatrix} \begin{pmatrix} \hat{a}_p \\ \hat{a}_s^\dagger \end{pmatrix} + i\hat{\mathbb{N}}_R \begin{pmatrix} \hat{f}_p \\ \hat{f}_s^\dagger \end{pmatrix} + i\hat{\mathbb{N}}_I \begin{pmatrix} \hat{f}_p^\dagger \\ \hat{f}_s \end{pmatrix}, \quad (7)$$

where $\hat{\mathbb{N}}_R + i\hat{\mathbb{N}}_I = \sqrt{2} \begin{pmatrix} \text{Re}(\alpha) & \text{Im}(\kappa) \\ -\text{Im}(\kappa) & 0 \end{pmatrix}$ are the noise matrices

and $\hat{f}_{p,s}$ denotes the Langevin noise operators⁴¹ (see the supplementary material for more details). Assuming the residual absorption insignificant, we can solve Eq. (7) and obtain the gain matrix for the mean amplitudes in the form of Eq. (4). We can then solve the propagation equations for quantum operators and obtain the differential photon-number variance in terms of the gain coefficients $|A|$ and $|C|$,

$$\text{Var}(\hat{n}_s - \hat{n}_p) = (|A|^2 - |C|^2) \langle \hat{n}_p(0) \rangle + \langle L_N \rangle, \quad (8)$$

where $\langle \hat{n}_p(0) \rangle$ and $\langle L_N \rangle$, respectively, denote the mean photon number of the seeding probe field and the grouped Langevin noise contributions (see the supplementary material for more details).

In the ideal lossless case ($|A|^2 - |C|^2 = 1$) without additional noise terms, Eq. (8) matches Eq. (6) as $\langle \hat{n}_p \rangle + \langle \hat{n}_s \rangle = (|A|^2 + |C|^2) \langle \hat{n}_p(0) \rangle$. However, higher N enhances probe-field optical loss, leading to increased excess noise (with super-Poisson statistics) in both probe and Stokes fields and, hence, prevents further squeezing improvements. Moreover, small imbalanced detector losses for the probe and Stokes channels ($\eta_p = 78\%$ and $\eta_s = 83\%$, respectively) further shift the conditions for optimal detectable squeezing further toward lower temperature (atomic density). Eventually, relative-intensity noise exceeds the shot-noise level, as depicted by the dotted and solid curves in Fig. 1(f). In the case of perfectly balanced detection, better squeezing level can be achieved at a higher atomic density. As a side note, one can notice that for low FWM gain, slightly higher detection losses for the probe field compensate for unity gain difference between probe and Stokes fields and allow for minuscule improvement in the detected squeezing. Overall, we observe reasonable agreement between the experimentally and theoretically predicted squeezing density dependence. The overall ≈ 2 dB difference between the measured and calculated noise level is observed. We can attribute it to experimental imperfections, including laser drifts, beam self-focusing, and residual pump field leakage. Additionally, other parasitic nonlinear effects, such as self-focusing or alternative wave-mixing channels, can emerge at higher atomic densities. Nevertheless, the model achieves a reasonably accurate prediction for the overall squeezing trend. This preliminary study is focused within the anti-PT symmetric region, since accurate measurement of quantum noise deviations from the shot noise in the low-gain regime was not possible due to technical noises, such as detector dark noise.

The pump laser power is another experimental parameter that we can use to control the FWM strength. For sufficiently powerful pump field, the FWM gain is independent of the pump laser intensity, but for weaker pump, this approach holds potential advantages for much faster tuning across the anti-PT EP, compared to the temperature tuning of the atomic density. Unfortunately, the reduction in the pump power generally results in higher optical losses. Figure 2 compares the simulation and experimental results of the pump power dependence. While the experimental normalized gain and measured squeezing align well with the simulations, it is clear that, at lower laser powers, the calculated eigenvalues deviate more substantially from the ideal expectations ($\text{Re}(\pm\lambda) = 0$ above the EP and $\text{Im}(\pm\lambda) = 0$ below the EP).

To demonstrate the capability of our proposed system in simulating near-perfect anti-PT Hamiltonian, we employ the developed numerical model to identify the required experimental conditions, as shown in Fig. 3. We find that operating at sufficiently large one-photon detuning $\Delta_1 \leq 4$ GHz provides necessary reduction in residual loss. However, to achieve necessary FWM gain, one will have to operate at higher cell temperature ($\geq 120^\circ\text{C}$) and greater pump laser power than what was available in the current experiments. Under these conditions, the calculated eigenvalues become symmetric and switch from almost entirely real to predominantly imaginary at the EP. For a longer vapor cell ($z = 7.6$ cm), $\pm\lambda z$ attains sufficient magnitude to enable relative oscillation in the normalized gain plot within the anti-PT symmetry breaking region. The negligible optical losses make it possible to observe corresponding variations in relative-intensity noise below the EP,²⁵ under certain conditions even dipping below the shot-noise level. Realization of this regime will allow us to explore the alternative mechanisms for quantum enhancement related to extreme

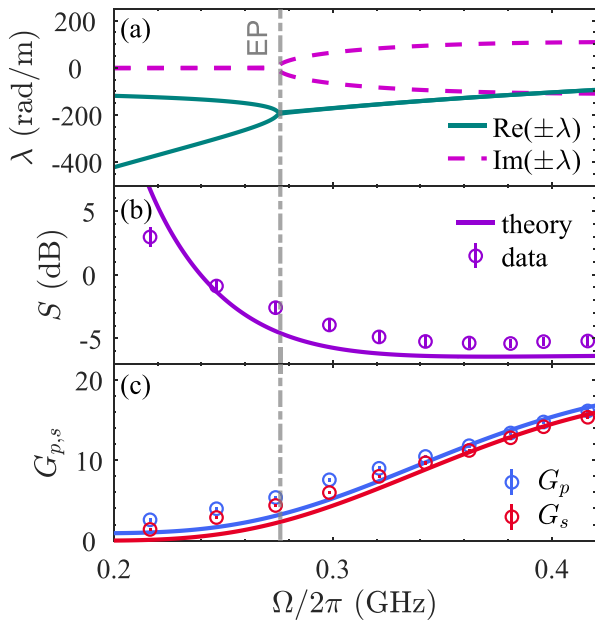


FIG. 2. System tuning across anti-PT symmetric and symmetry-breaking regimes via pump laser power modulation. (a) Simulated eigenvalues $\pm\lambda$ of the anti-PT Hamiltonian vs pump Rabi frequency Ω . Power dependences of (b) the relative-intensity squeezing parameter S and (c) normalized probe/Stokes gain $G_{p,s}$; markers represent experimental measurements and lines represent numerical simulations. Experimental parameters, also used for the numerical model: $\Delta = 0.7$ GHz, $\delta = -28$ MHz, $N = 7.9 \times 10^{12} \text{ cm}^{-3}$ (atomic vapor temperature $\sim 108^\circ\text{C}$), and $\Delta k = 210$ rad/m.

sensitivity of the system near the EP in addition to a more traditional benefits of high two-mode intensity squeezing above EP. Previous theoretical analysis predicts that operating near the EP enables optimal quantum sensing, even when low FWM gain produces negligible amount of intensity squeezing. Luo *et al.*³¹ proved that by comparing the inverse variance (akin to the Cramer–Rao bound) with the corresponding quantum Fisher information and showing that they converge in the ideal case. However, under the same parametric gain, traditional squeezing-based sensing deviates significantly from the quantum Fisher information, indicating suboptimal performance, and it requires significantly higher parametric gain to also saturate the quantum Fisher information.⁴³

It is important to note that complete elimination of the Langevin noise contributions proves to be challenging. Although in an ideal lossless scenario, squeezing continually improves with N , our model predicts that even under more favorable conditions, the inescapable optical losses will cause rapid squeezing degradation above certain atomic density, as shown in Fig. 3(c). Operating at larger laser detuning only pushes this optimal squeezing point to higher atomic densities (compare, e.g., the horizontal scales in Figs. 1 and 3). Nevertheless, in the vicinity of the EP, the ability to reproduce rapidly changing quantum squeezing behavior, as identified in Ref. 31, remains feasible. Thus, the extension of the original quantum Fisher information analysis accounting for optical loss and Langevin noise remains an open question for future theoretical and experimental works.

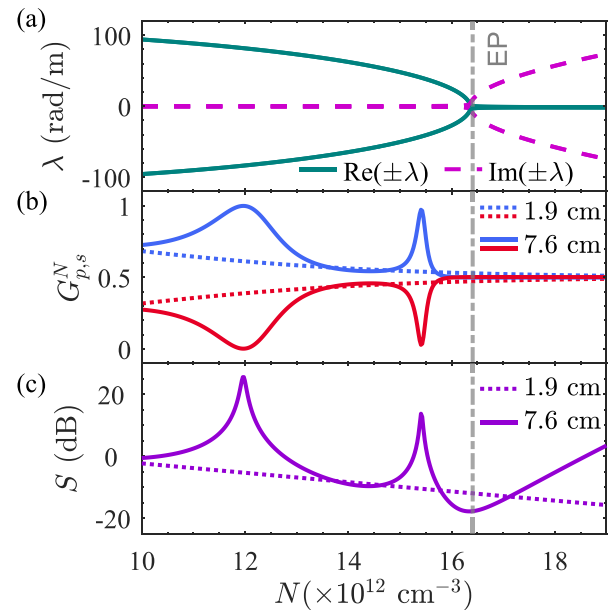


FIG. 3. Optimized FWM parameters for nearly ideal anti-PT realizations, using higher pump power ($\Omega = 2\pi \times 0.6$ GHz) and larger one-photon detuning ($\Delta_1 = 4$ GHz), in $z = 1.9$ and $z = 7.6$ cm vapor cells. Additional parameters: $\delta = -3.5$ MHz and $\Delta k = 210$ rad/m. (a) Real/imaginary components of the eigenvalues as functions of the atomic density N . (b) Normalized probe/Stokes gain vs N . (c) Relative-intensity squeezing parameter S vs N . Solid/dashed lines show the predicted squeezing with the Langevin noise $\langle L_N \rangle$ at a $z = 7.6/1.9$ cm vapor cell, respectively. No detector losses are considered.

In conclusion, our preliminary work establishes the practicality of modeling the anti-PT symmetric Hamiltonian by utilizing two correlated optical fields generated through the near-resonant forward FWM process in hot Rb atoms, particularly for studies of its quantum properties. We demonstrated that it is possible to tune the interaction parameters across the anti-PT phase transition and verified that both classical and quantum behaviors of the probe and Stokes fields exhibit the expected characteristics below and above the exceptional point. Namely, we observe two-mode relative-intensity squeezing at the anti-PT symmetric regime, when both output fields experience matching exponential FWM gain. We also analyze the influence of excess noise resulting from residual optical absorption, which imposes constraints on the attainable level of squeezing in distinct domains. Finally, we identified reasonable experimental parameters for observation of the nearly lossless oscillatory behavior, which can be applied for further advancing quantum sensor applications.

See the supplementary material for a comprehensive analysis and experimental specifics.

This work was supported by the Department of Energy (Grant No. DE-SC0022069). C.Z. acknowledges support from the National Science Foundation (Nos. PHY-2110212 and OMR-2228725). Z.N. and I.N. thank R. Behary and E.E. Mikhailov for their help with the experiment.

AUTHOR DECLARATIONS

Conflict of Interest

The authors have no conflicts to disclose.

Author Contributions

Ziqi Niu: Data curation (lead); Formal analysis (lead); Investigation (lead); Methodology (lead); Software (lead); Validation (lead); Visualization (lead); Writing – original draft (lead); Writing – review & editing (equal). **Yue Jiang:** Data curation (equal); Formal analysis (equal); Methodology (equal); Software (equal); Validation (equal); Visualization (equal); Writing – review & editing (equal). **Jianming wen:** Conceptualization (equal); Funding acquisition (equal); Investigation (equal); Methodology (equal); Project administration (equal); Resources (equal); Supervision (equal); Validation (equal); Writing – review & editing (equal). **Chuanwei Zhang:** Conceptualization (equal); Project administration (equal); Supervision (equal); Writing – review & editing (equal). **Shengwang Du:** Conceptualization (equal); Formal analysis (equal); Funding acquisition (equal); Investigation (equal); Methodology (equal); Project administration (equal); Resources (equal); Supervision (equal); Validation (equal); Writing – review & editing (equal). **Irina Novikova:** Conceptualization (equal); Data curation (equal); Formal analysis (equal); Funding acquisition (equal); Investigation (equal); Methodology (equal); Project administration (lead); Resources (lead); Software (equal); Supervision (lead); Validation (equal); Visualization (equal); Writing – original draft (lead); Writing – review & editing (lead).

DATA AVAILABILITY

The data that support the findings of this study are available from the corresponding author upon reasonable request.

REFERENCES

- ¹C. M. Bender and S. Boettcher, “Real spectra in non-Hermitian Hamiltonians having PT symmetry,” *Phys. Rev. Lett.* **80**, 5243 (1998).
- ²C. M. Bender, “Making sense of non-Hermitian Hamiltonians,” *Rep. Prog. Phys.* **70**, 947 (2007).
- ³R. El-Ganainy, K. G. Makris, M. Khajavikhan, Z. H. Musslimani, S. Rotter, and D. N. Christodoulides, “Non-Hermitian physics and PT symmetry,” *Nat. Phys.* **14**, 11–19 (2018).
- ⁴L. Ge and H. E. Türeci, “Antisymmetric PT-photonic structures with balanced positive- and negative-index materials,” *Phys. Rev. A* **88**, 053810 (2013).
- ⁵H. Fan, J. Chen, Z. Zhao, J. Wen, and Y.-P. Huang, “Antiparity-time symmetry in passive nanophotonics,” *ACS Photonics* **7**, 3035–3041 (2020).
- ⁶W. Chen, Ş. Kaya Özdemir, G. Zhao, J. Wiersig, and L. Yang, “Exceptional points enhance sensing in an optical microcavity,” *Nature* **548**, 192–196 (2017).
- ⁷J. Wiersig, “Review of exceptional point-based sensors,” *Photonics Res.* **8**, 1457–1467 (2020).
- ⁸J. M. P. Nair, D. Mukhopadhyay, and G. S. Agarwal, “Enhanced sensing of weak anharmonicities through coherences in dissipatively coupled anti-PT symmetric systems,” *Phys. Rev. Lett.* **126**, 180401 (2021).
- ⁹M. De Carlo, “(INVITED) Exceptional points of parity-time-and anti-parity-time-symmetric devices for refractive index and absorption-based sensing,” *Results Opt.* **2**, 100052 (2021).
- ¹⁰C. Wang, Z. Fu, W. Mao, J. Qie, A. D. Stone, and L. Yang, “Non-Hermitian optics and photonics: From classical to quantum,” *Adv. Opt. Photonics* **15**, 442–523 (2023).
- ¹¹D. Christodoulides and J. Yang, *Parity-Time Symmetry and Its Applications* (Springer, 2018), Vol. 280.
- ¹²Ş. K. Özdemir, S. Rotter, F. Nori, and L. Yang, “Parity-time symmetry and exceptional points in photonics,” *Nat. Mater.* **18**, 783–798 (2019).
- ¹³P. Peng, W. Cao, C. Shen, W. Qu, J. Wen, L. Jiang, and Y. Xiao, “Anti-parity-time symmetry with flying atoms,” *Nat. Phys.* **12**, 1139–1145 (2016).
- ¹⁴L. Feng, Z. J. Wong, R.-M. Ma, Y. Wang, and X. Zhang, “Single-mode laser by parity-time symmetry breaking,” *Science* **346**, 972–975 (2014).
- ¹⁵S. Yu, Y. Meng, J.-S. Tang, X.-Y. Xu, Y.-T. Wang, P. Yin, Z.-J. Ke, W. Liu, Z.-P. Li, Y.-Z. Yang *et al.*, “Experimental investigation of quantum PT-enhanced sensor,” *Phys. Rev. Lett.* **125**, 240506 (2020).
- ¹⁶S. Longhi, “Bloch oscillations in complex crystals with PT symmetry,” *Phys. Rev. Lett.* **103**, 123601 (2009).
- ¹⁷L. Ge, Y. D. Chong, S. Rotter, H. E. Türeci, and A. D. Stone, “Unconventional modes in lasers with spatially varying gain and loss,” *Phys. Rev. A* **84**, 023820 (2011).
- ¹⁸M. H. Teimourpour, L. Ge, D. N. Christodoulides, and R. El-Ganainy, “Non-Hermitian engineering of single mode two dimensional laser arrays,” *Sci. Rep.* **6**, 33253 (2016).
- ¹⁹M. P. Hokmabadi, N. S. Nye, R. El-Ganainy, D. N. Christodoulides, and M. Khajavikhan, “Supersymmetric laser arrays,” *Science* **363**, 623–626 (2019).
- ²⁰M. Zhang, W. Sweeney, C. W. Hsu, L. Yang, A. D. Stone, and L. Jiang, “Quantum noise theory of exceptional point amplifying sensors,” *Phys. Rev. Lett.* **123**, 180501 (2019).
- ²¹M. Naghiloo, M. Abbasi, Y. N. Joglekar, and K. W. Murch, “Quantum state tomography across the exceptional point in a single dissipative qubit,” *Nat. Phys.* **15**, 1232–1236 (2019).
- ²²Y. Li, Y.-G. Peng, L. Han, M.-A. Miri, W. Li, M. Xiao, X.-F. Zhu, J. Zhao, A. Alü, S. Fan *et al.*, “Anti-parity-time symmetry in diffusive systems,” *Science* **364**, 170–173 (2019).
- ²³A. Bergman, R. Duggan, K. Sharma, M. Tur, A. Zadok, and A. Alü, “Observation of anti-parity-time-symmetry, phase transitions and exceptional points in an optical fibre,” *Nat. Commun.* **12**, 486 (2021).
- ²⁴M. Jasperse, “Relative intensity squeezing: By four-wave mixing in rubidium,” Masters thesis (University of Melbourne, School of Physics, 2010).
- ²⁵Y. Jiang, Y. Mei, Y. Zuo, Y. Zhai, J. Li, J. Wen, and S. Du, “Anti-parity-time symmetric optical four-wave mixing in cold atoms,” *Phys. Rev. Lett.* **123**, 193604 (2019).
- ²⁶C. F. McCormick, A. M. Marino, V. Boyer, and P. D. Lett, “Strong low-frequency quantum correlations from a four-wave-mixing amplifier,” *Phys. Rev. A* **78**, 043816 (2008).
- ²⁷V. Boyer, A. M. Marino, R. C. Pooser, and P. D. Lett, “Entangled images from four-wave mixing,” *Science* **321**, 544–547 (2008).
- ²⁸B. J. Lawrie, P. D. Lett, A. M. Marino, and R. C. Pooser, “Quantum sensing with squeezed light,” *ACS Photonics* **6**, 1307–1318 (2019).
- ²⁹M.-C. Wu, B. L. Schmittberger, N. R. Brewer, R. W. Speirs, K. M. Jones, and P. D. Lett, “Twin-beam intensity-difference squeezing below 10 Hz,” *Opt. Express* **27**, 4769–4780 (2019).
- ³⁰N. Prajapati and I. Novikova, “Polarization-based truncated SU(1,1) interferometer based on four-wave mixing in Rb vapor,” *Opt. Lett.* **44**, 5921–5924 (2019).
- ³¹X.-W. Luo, C. Zhang, and S. Du, “Quantum squeezing and sensing with pseudo-anti-parity-time symmetry,” *Phys. Rev. Lett.* **128**, 173602 (2022).
- ³²H.-K. Lau and A. A. Clerk, “Fundamental limits and non-reciprocal approaches in non-Hermitian quantum sensing,” *Nat. Commun.* **9**, 4320 (2018).
- ³³B. E. Anderson, B. L. Schmittberger, P. Gupta, K. M. Jones, and P. D. Lett, “Optimal phase measurements with bright- and vacuum-seeded SU(1,1) interferometers,” *Phys. Rev. A* **95**, 063843 (2017).
- ³⁴N. Prajapati, Z. Niu, and I. Novikova, “Quantum-enhanced two-photon spectroscopy using two-mode squeezed light,” *Opt. Lett.* **46**, 1800–1803 (2021).
- ³⁵R. C. Pooser, N. Savino, E. Batson, J. L. Beckey, J. Garcia, and B. J. Lawrie, “Truncated nonlinear interferometry for quantum-enhanced atomic force microscopy,” *Phys. Rev. Lett.* **124**, 230504 (2020).
- ³⁶X. Liang, Z. Yu, C.-H. Yuan, W. Zhang, and L. Chen, “Phase sensitivity improvement in correlation-enhanced nonlinear interferometers,” *Symmetry* **14**, 2684 (2022).
- ³⁷A. V. Gorshkov, T. Calarco, M. D. Lukin, and A. S. Sørensen, “Photon storage in Λ -type optically dense atomic media. IV. Optimal control using gradient ascent,” *Phys. Rev. A* **77**, 043806 (2008).

- ³⁸Q. Glorieux, R. Dubessy, S. Guibal, L. Guidoni, J.-P. Likforman, T. Coudreau, and E. Arimondo, "Double- Λ microscopic model for entangled light generation by four-wave mixing," *Phys. Rev. A* **82**, 033819 (2010).
- ³⁹M. D. Lukin, P. R. Hemmer, and M. O. Scully, "Resonant nonlinear optics in phase-coherent media," *Adv. At., Mol., Opt. Phys.* **42**, 347–386 (2000).
- ⁴⁰M. T. Turnbull, P. G. Petrov, C. S. Embrey, A. M. Marino, and V. Boyer, "Role of the phase-matching condition in nondegenerate four-wave mixing in hot vapors for the generation of squeezed states of light," *Phys. Rev. A* **88**, 033845 (2013).
- ⁴¹Y. Jiang, Y. Mei, and S. Du, "Quantum Langevin theory for two coupled phase-conjugated electromagnetic waves," *Phys. Rev. A* **107**, 053703 (2023).
- ⁴²N. Prajapati, N. Super, N. R. Lanning, J. P. Dowling, and I. Novikova, "Optical angular momentum manipulations in a four-wave mixing process," *Opt. Lett.* **44**, 739–742 (2019).
- ⁴³T. S. Woodworth, C. Hermann-Avigliano, K. W. C. Chan, and A. M. Marino, "Transmission estimation at the quantum Cramér-Rao bound with macroscopic quantum light," *EPJ Quantum Technol.* **9**, 38 (2022).